# Hydrogen Exchange and Hydration Dynamics in Gelatin Gels

**Fabian Vaca Chávez,[†] Erik Hellstrand, and Bertil Halle***

*Contribution from the Department of Biophysical Chemistry, Lund University, SE-22100 Lund, Sweden*

*Received: December 29, 2005; In Final Form: August 30, 2006*

Gelatin, derived from the collagen triple helix, is the most widely used functional biopolymer and a prototype for studies of physical gels. Gelatin gels have also served as models for soft biological tissue in efforts to elucidate the molecular basis of the magnetic relaxation phenomena that govern magnetic resonance image contrast. Yet, the microstructure, hydration, and magnetic relaxation behavior of gelatin gels are not well understood. To address these issues, we report here the water $^2$H and $^{17}$O magnetic relaxation dispersion (MRD) profiles from gelatin gels over wide ranges of resonance frequency and pH. For the global analysis of this extensive data set, we use a generalized relaxation theory that remains valid for arbitrarily slow molecular dynamics. The strong pH dependence in the $^2$H profiles can be rationalized quantitatively as the result of exchange with bulk water of labile hydrogens in gelatin side chains. The global analysis of the MRD data yields hydrogen-exchange rate constants, acid dissociation constants, and orientational order parameters in agreement with independent structural, thermodynamic, and kinetic data. The MRD analysis reveals a highly mobile hydration layer at the surface of the gelatin triple helix and a small number of trapped water molecules with residence times on the order of $10^{-8}$ s, presumably associated with structural defects and branch points in the gel. The MRD data also indicate that ∼20% of the gelatin residues belong to flexible polypeptide chains, rather than to rigid triple-helical segments. By identifying the molecular species and motions responsible for the $^2$H and $^{17}$O dispersion profiles, this study takes a significant step toward a quantitative understanding of water relaxation in aqueous gels and biological tissue.

## 1. Introduction

Collagen, the most abundant protein in animals, is the main protein component of connective tissues, such as tendon, skin, cartilage, and bone.[1−3] The collagen molecule is a rodlike triple helix of ∼3000 Å length and 14 Å diameter (Figure 1), built from three parallel, supercoiled polypeptide chains in polyproline-II-like conformation. Each chain consists of 330−340 Xaa-Yaa-Gly tripeptide repeats. The collagen triple helix is densely packed, with the glycines at the center and the side chains of the Xaa and Yaa residues exposed to solvent.[4−7] In mammalian collagens, ∼20% of these residues are proline or hydroxyproline (Hyp) imino acids. It has been argued that Hyp stabilizes the triple helix by participating in H-bonded water chains bridging the Hyp hydroxyl of one strand with the backbone carbonyl of the same or another strand,[3,5,8,9] but this view has been challenged.[7,10]

Type B gelatin is produced by partial alkaline hydrolysis of collagen, leading to a polydisperse mixture of polypeptide chains with an average molecular weight of 40−90 kDa, compared to ∼100 kDa for intact collagen α-chains, and a low isoionic point of 4.8−5.2.[11] In aqueous solution above 40 °C, gelatin molecules behave as semiflexible coils, but at 30−35 °C the solution undergoes a sol−gel transition.[12,13] Gelatin gels are built from collagen-like triple-helical junction zones, 100−200 residues in length, connected by flexible single chains and with many dangling single-strand ends.[2,14−16] The lateral aggregation[1] of gelatin triple helices that gives rise to collagen fibrils in vivo does not occur in gelatin gels.[12−14,17] Essentially all Xaa and Yaa side chains in a gelatin gel are thus solvent-exposed.

**Figure 1.** Triple-helical fragment of the collagen-like peptide $(PHG)_4EKG(PHG)_5$, based on heavy-atom coordinates from the X-ray crystal structure[6] (PDB file 1QSU) and hydrogen atoms added in standard geometry. Hydroxyl hydrogens in Hyp residues are colored yellow.

Gelatin is the most widely used functional biopolymer and has served as a prototype for studies of physical gels for decades.

* Address correspondence to this author. E-mail: bertil.halle@bpc.lu.se. Telephone: +46-46 222 9516. Fax: +46-46 222 4543.

[†] Present address: Institut für Physikalische Chemie, Universität Münster, DE-48149 Münster, Germany.

10.1021/jp057567s CCC: $33.50 
Published on Web 10/10/2006

Yet, many fundamental questions about molecular structure and dynamics in native gelatin gels are still unresolved. In particular, the hydration of the triple helix remains a controversial issue.[3,5−10,18] The magnetic relaxation dispersion (MRD) of the quadrupolar water isotopes $^2$H and $^{17}$O has been used extensively to study hydration and hydrogen exchange for globular proteins in aqueous solution.[19−22] In solutions of freely tumbling proteins, the frequency dependence of the longitudinal magnetic relaxation rate, known as the dispersion profile, is usually governed by protein rotational diffusion. In a gel with rotationally immobilized macromolecules, it is instead the exchange of trapped water molecules and labile hydrogens in amino acid side chains that produces the relaxation dispersion. Because these exchange processes may be slow compared to the nuclear couplings that they modulate, the magnetic relaxation behavior cannot be described by the conventional perturbation theory of nuclear spin relaxation.[23] Instead, a more general, nonperturbative theory must be used.[24]

Here, we report the first water $^2$H/$^{17}$O MRD study of gelatin gels, with MRD data covering five frequency decades (for $^2$H) and a wide range of pH values. Using the generalized relaxation theory,[24] we demonstrate that the strong observed pH dependence in the $^2$H dispersion profiles can be quantitatively accounted for in terms of the known amino acid composition and the expected hydrogen exchange rate constants and acid dissociation constants. The analysis also sheds new light on the hydration and microstructure of native gelatin gels. By identifying the molecular species and motions responsible for the $^2$H and $^{17}$O dispersion profiles, this study provides essential benchmarks for the analysis (complicated by dipolar cross-relaxation effects) of the $^1$H dispersion profiles from the same gelatin gels.[25] Because aqueous biopolymer gels and soft biological tissue display similar magnetic relaxation behavior, a quantitative understanding of the $^1$H dispersion profiles from biopolymer gels will also help to unravel the molecular basis of relaxation-induced contrast in clinical magnetic resonance imaging.[26−33]

## 2. Materials and Methods

**2.1. Gel Preparation.** Gelatin type B from bovine skin was obtained from Sigma (product no. G9382, lot no. 053H0271) and was used as supplied. A complete amino acid analysis was performed on this gelatin preparation, with results (Table 1) in good agreement with the expected relative amino acid composition. In particular, the glycine content of 33.5 mol % closely matches the expected 33.3%. The total amino acid content was 77.1%, slightly lower than the 81% specified by the manufacturer. The mean residue molar mass calculated from the composition in Table 1 is 91.04 g mol$^{-1}$. According to the manufacturer, this gelatin preparation has a Bloom number of ∼225, corresponding to an average molecular weight of ∼50 kDa, or ∼550 residues.

All MRD samples contained 10.0 wt % gelatin in water. The $^2$H MRD sample was made from $D_2O$ with 99.9 at. % $^2$H and low paramagnetic content (Cambridge Isotope Laboratories), and the $^{17}$O MRD sample, from a 50:50 wt % mixture of $D_2O$ and $H_2O$ with 19.2 at. % $^{17}$O (Isotec). As a measure of gelatin concentration, we use the number, $N_T$, of water molecules per average amino acid residue (with molar mass 91.04 g mol$^{-1}$). In calculating $N_T$, we made a small correction for the nonprotein fraction of the gelatin preparation (see above), assumed to be water. The $N_T$ values were 54.6 and 57.5 for the $^2$H and $^{17}$O MRD samples, respectively. All relaxation data presented here have been normalized to $N_T = 60$, based on the expected inverse proportionality between $R_1 - R_1^{(0)}$ and $N_T$ (section 2.3). Here, $R_1^{(0)} = 3.67$ s$^{-1}$ ($^2$H) or 249.7 s$^{-1}$ ($^{17}$O) is the relaxation rate measured at 10 °C on a pure water reference sample of the same isotopic composition as in the gelatin samples.

**TABLE 1: Amino Acid Composition of Gelatin Preparation**

| residue | mol % | $N_k^{0a}$ |
|---|---|---|
| Gly | 33.5 | |
| Pro | 12.7 | |
| Ala | 10.8 | |
| Hyp | 8.8 | 0.044 |
| Glu | 7.4 | 0.037 |
| Arg | 4.9 | 0.122[b] |
| Asp | 4.6 | 0.023 |
| Ser | 3.8 | 0.019 |
| Lys | 2.6 | 0.040 |
| Leu | 2.4 | |
| Val | 2.1 | |
| Thr | 1.7 | 0.008 |
| Phe | 1.2 | |
| Ile | 1.1 | |
| Met | 0.6 | |
| Hyl | 0.6 | 0.003+0.009 |
| His | 0.5 | 0.002 |
| Tyr | 0.4 | 0.002 |
| other | 0.3 | |
| COOH | 12.0 | 0.060 |
| OH | 15.4 | 0.076 |
| NH | 8.6 | 0.173 |
| labile | 36.0 | 0.309 |

[a] Number of labile-H water equivalents per average amino acid residue, $N_k^0 = (n_k/2) \times$ (mol %/100), $n_k$ = number of labile H in residue $k$. [b] 4 $\eta$-NH and 1 $\epsilon$-NH.

The gels were prepared by dissolving gelatin in water at 60 °C, yielding a clear solution of pH* 5.4. For samples at other pH* values, microliter amounts of 0.1 M HCl or 0.5 M NaOH were added. Portions (∼1 mL) of this solution were transferred to 10 mm O.D. NMR tubes, and the temperature was reduced to 40 °C, where pH* was measured (pH* refers to the operational pH value, not corrected for H/D isotope effects). The samples were then cooled below the sol→gel transition, which occurred between 25 and 30 °C, and were stored at 15 °C for at least 16 h before MRD measurements.

**2.2. MRD Experiments.** The longitudinal relaxation rate, $R_1$, of the water $^2$H magnetization was measured over five frequency decades, from 1.4 kHz to 92 MHz. To cover this frequency range, we used six different NMR spectrometers: (1) a Stelar Spinmaster fast field-cycling (FC) spectrometer (1.4 kHz−1.5 MHz); (2) a field-variable iron-core magnet equipped with a Tecmag console (2.2−10.5 MHz); and (3) Bruker Avance DMX 100 and 200 spectrometers and Varian Unity 500 and 600 spectrometers with conventional cryomagnets (15.4, 30.7, 76.8, and 92.2 MHz). $R_1$ of the water $^{17}$O magnetization was measured over two frequency decades, 1.1−81 MHz, using the Tecmag system (1.1−9.8 MHz) and conventional spectrometers (13.6, 27.1, 67.8, and 81.3 MHz). The temperature was maintained at 10.0 ± 0.1 °C and was checked with a thermocouple referenced to an ice−water bath. All MRD measurements were completed within 2 weeks of sample preparation.

The FC technique overcomes the sensitivity problem of conventional fixed-field experiments in weak magnetic fields.[34,35] For FC experiments on $^2$H, we used a CPMG detection sequence with a 90° pulse length of 19.5 $\mu$s and a 180° pulse spacing of 120 $\mu$s. The polarization and detection frequencies were 3.07 and 2.98 MHz, respectively. At higher frequencies, $R_1$ was measured with the $180° - \tau - 90°$ inversion recovery sequence for both $^2$H and $^{17}$O. Single-exponential recovery curves were

obtained throughout, from which $R_1$ was determined by a three-parameter fit.

**2.3. Analysis of MRD Data.** The relaxation of the longitudinal $^2$H or $^{17}$O magnetization is caused by thermal fluctuations of the nuclear quadrupole−electric field gradient interaction of water nuclei ($^2$H or $^{17}$O) or labile deuterons in amino acid side chains ($^2$H).[23] Relaxation is induced by molecular motions that randomize the orientation of the field gradient tensor. Under the conditons of the present study, the observed longitudinal $^2$H or $^{17}$O relaxation rate can be expressed as[24,33]

$$R_1(\omega_0) = (1 - \sum_k f_k)R_1^{(0)} + \sum_k f_k R_1^{(k)}(\omega_0) \qquad (1)$$

where $\omega_0 = 2\pi\nu_0$ is the angular Larmor frequency and $f_k$ is the fraction of deuterons or oxygen-17 nuclei in environment $k$:

$$f_k = \frac{N_k}{N_T} \qquad (2)$$

Here, $N_k$ is either the average number of long-lived water molecules of type $k$ per amino acid residue or the average number of labile deuterons divided by 2 (the number of water equivalents) of type $k$ per residue (Table 1). The latter contribution only occurs for $^2$H relaxation, of course. Further, $N_T$ is the total number of water molecules per average amino acid residue. The labile-deuteron contribution to $N_T$ never exceeds 0.3 (Table 1) and can therefore be neglected.

Equation 1 is formally identical to the result obtained in the fast-exchange limit for a multiphase system. When the system is dilute ($f_k \ll 1$) and the quadrupole coupling is orientationally randomized by the exchange process itself, as is the case here, then eq 2 is actually valid for all exchange rates. However, as shown elsewhere,[24] the intrinsic $^2$H relaxation rate in environment $k$ must then be expressed as

$$R_1^{(k)}(\omega_0) = \frac{2}{3}\Omega_{Q,k}^2[0.2\,\tilde{J}^{(k)}(\omega_0) + 0.8\,\tilde{J}^{(k)}(2\omega_0)] \qquad (3)$$

with the generalized spectral density function

$$\tilde{J}^{(k)}(m\omega_0) = \frac{\tau_k}{1 + (\omega_{k,m}^{\text{eff}}\tau_k)^2} \qquad (4)$$

and the effective frequency

$$\omega_{k,m}^{\text{eff}} = [\Omega_{Q,k}^2 + (m\omega_0)^2]^{1/2} \qquad (5)$$

The Lorentzian form of the effective spectral density function in eq 4 is a consequence of the complete orientational randomization brought about by exchange.[24,33] The residual $^2$H quadrupole frequency appearing in eqs 3 and 5 is defined as

$$\Omega_{Q,k} = \frac{3\pi}{2}S_k\chi_k \qquad (6)$$

The $^2$H field gradient tensor is very nearly axially symmetric, with the principal component along the O−D or N−D bond. For the rigid-lattice quadrupole coupling constant, $\chi$, we use the value 226 kHz for deuterons in water molecules and 212 kHz (OD) or 180 kHz (ND) for labile gelatin deuterons.[21,36] Subpicosecond librations and subnanosecond local rotation of O−D and N−D vectors do not contribute directly to the observed relaxation dispersion, but scale the quadrupole interaction so that slower motions modulate a residual quadrupole coupling, $S\chi$, where $S$ is the rank-2 orientational order parameter.[21]

In the motional narrowing regime, where $(\Omega_{Q,k}\tau_k)^2 \ll 1 + (\omega_0\tau_k)^2$, eq 4 reduces to the usual spectral density, $J^{(k)}(m\omega_0) = \tau_k/[1 + (m\omega_0\tau_k)^2]$. (Some authors prefer a definition of the spectral density function that differs from ours by a factor of 2. Alternatively, this factor may be included in eq 3, as we have done.) This limit is applicable for the water contribution to $R_1$ for both $^2$H and $^{17}$O. The $^{17}$O data can therefore be described with the usual dispersion law,[21] corresponding to eqs 1−4 with $\omega_{k,m}^{\text{eff}} = m\omega_0$ and $\Omega_{Q,k} = \sqrt{18/125}\,\pi S_k\chi_k$. For $^{17}$O in water, we use an effective quadrupole coupling constant $\chi = 7.8$ MHz (including the effect of field gradient asymmetry).[21]

To reduce the number of model parameters, the 11 types of labile gelatin deuteron (Table 1) are reduced to three classes: COOD (Asp, Glu), OD (Hyp, Ser, Thr, Hyl, Tyr), and ND (Arg, Lys, Hyl, His). For the COOD class, deuteron exchange occurs directly to water with a pH-independent labile-deuteron residence time $\tau_{\text{COOD}}$.[37,38] Since this is longer than the water residence times (see below), we use the generalized spectral density in eq 4. The fraction $f_{\text{COOD}}$ is obtained from eq 2 with

$$N_{\text{COOD}} = \frac{N_{\text{COOD}}^0}{1 + 10^{\text{pD}-\text{p}K_{\text{COOD}}}} \qquad (7)$$

where[39] pD = pH* + 0.41 and $N_{\text{COOD}}^0 = 0.060$ is the average number of carboxyl groups divided by two (i.e., the number of water equivalents) per residue (Table 1).

For the OD class, deuteron exchange occurs directly to water and by acid or base-catalyzed mechanisms. The mean residence time, $\tau_{\text{OD}}$, of hydroxyl deuterons is thus given by

$$\frac{1}{\tau_{\text{OD}}} = k_0^{\text{OD}} + k_1^{\text{OD}}\,10^{-\text{pD}} + k_2^{\text{OD}}\,10^{\text{pD}-\text{p}K_W} \qquad (8)$$

where $\text{p}K_W = 15.53$ is the ionization constant of $D_2O$ at 10 °C.[40] At any given pD value, at most two of the three terms in eq 8 contribute significantly. For the OD class, $(\omega_{k,m}^{\text{eff}}\,\tau_k)^2 \gg 1$ at all investigated pD values and frequencies. In this slow-exchange regime, eqs 3−5 yield

$$R_1^{(k)}(\omega_0) = \frac{2}{3\tau_k}\left[\frac{0.2}{1 + (\omega_0/\Omega_{Q,k})^2} + \frac{0.8}{1 + (2\omega_0/\Omega_{Q,k})^2}\right] \qquad (9)$$

The dispersion profile still has a Lorentzian shape, but the dispersion frequency is now the quadrupole frequency $\Omega_{Q,k}$ rather than the inverse correlation time. In the slow-exchange regime, molecular motions thus have no effect on the dispersion frequency but only scale the amplitude of the dispersion step.

For the ND class, hydrogen exchange is base catalyzed and the mean residence time, $\tau_{\text{ND}}$, is given by

$$\frac{1}{\tau_{\text{ND}}} = \frac{k_2^{\text{ND}}}{n_{\text{ND}}}10^{\text{pD}-\text{p}K_W} \qquad (10)$$

since only one of the $n_{\text{ND}}$ equivalent deuterons is exchanged in each transfer event. We thus have $n_{\text{ND}} = 4$ for Arg $\eta$-ND, $n_{\text{ND}} = 1$ for Arg $\epsilon$-ND, and $n_{\text{ND}} = 3$ for Lys and Hyl $\zeta$-ND. Since we treat all these ND deuterons as a single class, we use a population-weighted value in eq 10: $n_{\text{ND}} = [4.87 \times (4 + 1)/2 + (2.64 + 0.60) \times 3]/(4.87 + 2.64 + 0.60) = 2.70$ (the contribution from His residues is negligible; see Table 1). The

fraction $f_{ND}$ is obtained from eq 2 with $N_{ND} = N^0_{ND,Arg} + N_{ND,Lys}$ and

$$N_{ND,Lys} = \frac{N^0_{ND,Lys}}{1 + 10^{pD - pK_{ND,Lys}}} \quad (11)$$

where $N^0_{ND,Arg} = 0.122$ and $N^0_{ND,Lys} = 0.049$ (Table 1). The acid dissociation constant $pK_{ND,Lys}$ in eq 11, which pertains to Lys and Hyl, is taken to be 11.1, based on the value[41] $pK_{NH,Lys} = 10.5$ (in $H_2O$ at 10 °C) and an H/D isotope effect[42] $pK_{ND,Lys} = pK_{NH,Lys} + 0.6$. The precise value used for $pK_{ND,Lys}$ is not critical since, according to eq 11, only 5% of the Lys residues are titrated even at the highest investigated pH* value of 9.4. Since, Hyl residues only make up 5% of the labile ND deuterons (Table 1), we neglect the fact that $pK_{NH}$ for Hyl is 0.8 units lower than that for Lys.[43] At the basic pD values where ND deuterons contribute significantly to $R_1$, $\tau_{ND}$ is of the same order of magnitude as $\tau_{OD}$ and we use the slow-exchange limit, eq 9, for both classes.

Because the gel contains rigid triple-helical segments as well as flexible single-strand segments, each of the three labile-deuteron contributions is a sum of two terms:

$$R_1^{(k)}(\omega_0) = x_{helix}\, R_1^{(k),helix}(\omega_0) + x_{strand}\, R_1^{(k),strand}(\omega_0) \quad (12)$$

where $x_{strand}$ and $x_{helix} = 1 - x_{strand}$ are the fraction residues in single-strand and triple-helical segments. The relaxation rate $R_1^{(k),helix}$ is given by eq 3 or 9, and $R_1^{(k),strand}$ is given by similar expressions with the only difference that $\Omega_{Q,k}$ is multiplied by the single-strand order parameter $S_{strand}$. The parameters $x_{strand}$ and $S_{strand}$ are the same for all three labile deuteron classes. The $^2H$ and $^{17}O$ water components (W1 and W2) should also be decomposed as in eq 12, but since extended single-strand segments cannot trap water molecules we expect that $R_1^{W,k,strand} = 0$. The only effect of the distribution of residues between triple-helical and single-strand segments is then to replace $N_{W,k}$ in eq 2 by $x_{helix}N_{W,k}$.

Fits to the dispersion profiles were made with the Levenberg–Marquardt algorithm[44] with equal weighting of all data points. Quoted uncertainties in parameter values (one standard deviation) were calculated with an estimated 1% accuracy in all $R_1$ values. The target function for the fit was eq 1, which may be written in the form

$$R_1(\omega_0) = \alpha + f_{W1}R_1^{W1}(\omega_0) + f_{W2}R_1^{W2}(\omega_0) + f_{COOD}R_1^{COOD}(\omega_0) + f_{OD}R_1^{OD}(\omega_0) + f_{ND}R_1^{ND}(\omega_0) \quad (13)$$

The first term, $\alpha$, represents all frequency-independent contributions to $R_1$, notably from the bulk water phase and from the mobile hydration layer at the surface of gelatin triple helices or single strands. An adequate description of the $^2H$ and $^{17}O$ MRD data requires two water correlation times, denoted W1 and W2. These are both in the motional-narrowing regime and are therefore described by two parameters each: $N_{W1}S^2_{W1}$ and $\tau_{W1}$, and similarly for component W2. The remaining terms in eq 13 refer to the three classes of labile deuteron, described by the generalized spectral density in the form of eqs 3 and 4 (COOD) or its slow-exchange limit, eq 9 (OD and ND). Because the ND contribution is negligibly small except at the two highest pH* values, the $^2H$ MRD data from the four lower pH* values were fitted jointly without this contribution. The COOD and OD contributions are then modeled by three parameters each: $S_{COOD}$, $\tau_{COOD}$, and $pK_{COOD}$ for the COOD class and $S_{OD}$, $k_0^{OD}$, and $k_1^{OD}$ for the OD class. The microstructure of the gel is modeled by the two pH-independent parameters $x_{strand}$ and $S_{strand}$. The two $^2H$ dispersion profiles at basic pH* values were fitted jointly without the COOD term (because all Asp and Glu side chains are ionized at these pH* values) and with all water and gel microstructure parameters fixed at the values deduced from the fit to the acidic dispersion profiles. The additional parameters are the base-catalyzed hydrogen exchange rate constants $k_2^{OD}$ and $k_2^{ND}$, the order parameter $S_{ND}$, and several parameters modeling internal motions in the flexible Arg and Lys side chains (section 3.4).

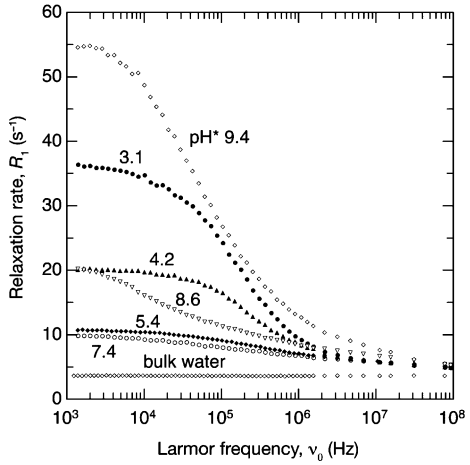


**Figure 2.** $^2H$ MRD profiles from gelatin gels at 10.0 °C and the indicated pH* values, all scaled to a concentration of 60 water molecules per amino acid residue. The frequency-independent $R_1$ values measured on a pure $D_2O$ reference sample are also shown.

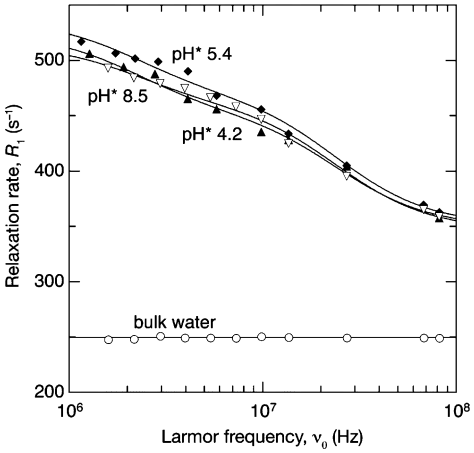


**Figure 3.** $^{17}O$ MRD profiles from gelatin gels at 10.0 °C and the indicated pH* values, all scaled to a concentration of 60 water molecules per amino acid residue. The frequency-independent $R_1$ values measured on a pure HDO reference sample are also shown. The dispersion curves resulted from separate bilorentzian fits with the two correlation times fixed at the values obtained from the $^2H$ profiles (see text).

## 3. Results and Discussion

**3.1. $^2H$ and $^{17}O$ MRD Profiles from Gelatin Gels.** Figures 2 and 3 show the water $^2H$ and $^{17}O$ $R_1$ dispersion profiles measured at 10.0 °C on identically prepared gelatin gels at several pH* values. Whereas the $^2H$ profiles depend strongly on pH, the $^{17}O$ profiles exhibit little or no pH dependence. This demonstrates that the pH dependence in the $^2H$ profiles is not due to a variation in the gel structure (which would also have shown up in the $^{17}O$ profiles). Rather, it is caused by pH-dependent exchange and ionization of amino acid side chains

with labile deuterons. In particular, the 5.5-fold increase of $R_1$ (at low frequencies) between pH* 7.4 and 9.4 must reflect base-catalyzed exchange of side-chain OD and ND deuterons. On the acidic side, $R_1$ increases by a factor 3.8 between pH* 7.4 and 3.1, reflecting acid-catalyzed deuteron exchange in hydroxyl groups as well as titration of carboxyl groups. Whereas the $^{17}O$ dispersion provides unequivocal evidence for the presence in the gelatin gel of water molecules with residence times longer than ~1 ns, these water molecules only contribute to the $^2H$ dispersion at high (>1 MHz) frequencies.

Because the $^{17}O$ profiles show little or no pH dependence (Figure 3), we may assume that the microstructure of the gel is the same at all investigated pH values. This means that the number of long-lived water molecules, their order parameters, and their residence times should be the same for all six $^2H$ profiles, thus reducing the number of adjustable parameters. Except for the order parameters, these water-related parameters should also be the same for the $^2H$ and $^{17}O$ dispersions. Furthermore, the fraction, $x_{strand}$, of residues in single-strand conformation (rather than triple helix) and the associated polypeptide chain order parameter, $S_{strand}$, should be the same for the two nuclei and at all pH values.

In modeling the pH dependence of the $^2H$ profiles, we group the different types of labile deuterons present in gelatin into three classes: COOD, OD, and ND (Sect. 2.3). Because exchange of ND deuterons is base-catalyzed, this class only contributes at the basic pH* values 8.6 and 9.4. On the other hand, the COOD class does not contribute at these pH* values, since all carboxyl groups are then ionized. It is therefore convenient to analyze the $^2H$ profiles in two groups. The four profiles at pH* 3.1, 4.2, 5.4, and 7.4 are fitted jointly with common parameters describing the COOD and OD classes, whereas the two profiles at pH* 8.6 and 9.4 are fitted jointly with common parameters for the OD and ND classes. The OD order parameter, $S_{OD}$, and the direct exchange rate constant, $k_0^{OD}$, are constrained to have the same values in the two fits.

**3.2. Exchange of COOD and OD Deuterons at Acidic and Neutral pH.** Figure 4a shows the result of a simultaneous fit of the model described in section 2.3 to the four $^2H$ profiles recorded at acidic and neutral pH* values (altogether 206 $R_1$ values). It is evident that the model can account for the pH-dependent shape of the dispersion profile. Although there are 13 free parameters (Table 2), the adjusted values of the 6 parameters associated with the COOD and OD labile-deuteron classes are fully consistent with independent structural, thermodynamic, and kinetic information (see below). Figure 4b shows the pH* 3.1 profile decomposed into water, carboxyl, and hydroxyl contributions. Above 2 MHz, $R_1$ is essentially due to long-lived water molecules. This contribution is discussed in connection with the $^{17}O$ profiles (section 3.3).

The frequency dependence in the $^2H$ profiles below 1 MHz is produced by deuteron exchange in carboxyl and hydroxyl groups. At pH* 3.1, COOD and OD groups each account for ~40% of the low-frequency $R_1$, while bulk and hydration water each account for ~10% (Figure 4b). With parameter values from Table 2 inserted into eq 6, we find that $(\Omega_{COOD}\,\tau_{COOD})^2 \approx 0.008 \ll 1$. This contribution is thus in the fast-exchange, or motional-narrowing, regime. In this regime, $R_1^{COOD,strand}(\omega_0)/R_1^{COOD,helix}(\omega_0) = S_{strand}^2 x_{strand}/(1 - x_{strand}) \approx 0.004$ (Table 2), so that only COOD groups in triple-helical segments make a significant contribution to $R_1$. For the OD contribution, $(\Omega_{OD}\,\tau_{OD})^2 \gg 1$ for both helix and strand segments, justifying our use of the slow-exchange expression, eq 9. In this regime, $R_1^{OD,strand}(0)/R_1^{OD,helix}(0) = x_{strand}/(1 - x_{strand}) \approx 0.3$ (Table 2), so that OD groups in single-strand segments do contribute, but with an apparent correlation time that is a factor $1/S_{strand} \approx 9$ longer than that for OD groups in triple-helical segments (13 versus 1.4 $\mu$s). In the acidic and neutral range, the pH dependence of the dispersion profiles is thus caused by variations in the amplitudes rather than in the (apparent) correlation times, all of which ($\tau_{W1}$, $\tau_{W2}$, $\tau_{COOD}$, and $1/\Omega_{OD}$) are independent of pH.

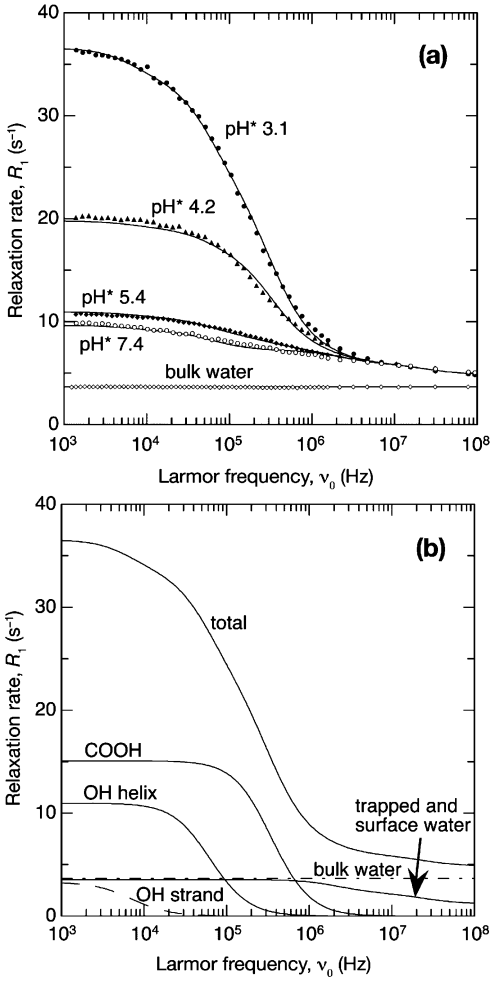


**Figure 4.** (a) $^2H$ MRD profiles from gelatin gels at 10.0 °C and the indicated acidic and neutral pH* values, all scaled to a concentration of 60 water molecules per amino acid residue. The dispersion curves resulted from a simultaneous fit to all data (see text). The parameter values resulting from the fit are given in Table 2. (b) Decomposition of the pH* 3.1 dispersion profile, showing the contributions from deuterons in hydration water molecules and in gelatin carboxyl (COOH) and hydroxyl (OH) groups.

**TABLE 2: Results of Simultaneous Fit to Four $^2H$ Profiles at pH* 3.1−7.4**

| parameter (unit) | value |
|---|---|
| $N_S(\langle\tau_S/\tau_{bulk}\rangle - 1)$ | $19.5 \pm 0.5$ |
| $N_{W1}S_{W1}^2$ | $(2.9 \pm 0.3) \times 10^{-2}$ |
| $\tau_{W1}$ (ns) | $3.6 \pm 0.4$ |
| $N_{W2}S_{W2}^2$ | $(3.5 \pm 0.3) \times 10^{-3}$ |
| $\tau_{W2}$ (ns) | $39 \pm 3$ |
| $pK_{COOD}$ | $4.75 \pm 0.01$ |
| $\tau_{COOD}$ ($\mu$s) | $0.26 \pm 0.01$ |
| $k_0^{OD}$ ($s^{-1}$) | $(2.8 \pm 0.1) \times 10^3$ |
| $k_1^{OD}$ ($M^{-1}\,s^{-1}$) | $(4.6 \pm 0.1) \times 10^7$ |
| $S_{COOD}$ | $0.35 \pm 0.01$ |
| $S_{OD}$ | $0.71 \pm 0.03$ |
| $S_{strand}$ | $0.11 \pm 0.02$ |
| $x_{strand}$ | $0.23 \pm 0.02$ |

The low-frequency COOD contribution to $R_1$ drops from 15 $s^{-1}$ at pH* 3.1, to 9 $s^{-1}$ at pH* 4.2, 1.3 $s^{-1}$ at pH* 5.4, and ~0 at pH* 7.4. This pH dependence is entirely due to acid dissociation, described by eq 7 with $pK_{COOD} = 4.75 \pm 0.01$ (Table 2). The H/D isotope effect on the dissociation of carboxylic acids[45] is $pK_{COOD} = pK_{COOH} + (0.50 \pm 0.02)$, so that the MRD-derived result corresponds to $pK_{COOH} = 4.25 \pm 0.02$. This value is intermediate between the standard $pK_a$ values for Asp (4.0) and Glu (4.4) side chains in oligopeptides.[46] (These values refer to 25 °C, but the temperature dependence of $pK_a$ is negligible for COOH groups.[41,47]) It is also consistent with the acidic part (pH 1.5−6.0) of the titration curve of gelatin.[41] The mean residence time of the COOD deuteron, $\tau_{COOD} = 0.26 \pm 0.01$ $\mu$s, derived from the $^2$H MRD profiles is in the expected range. For acetic and malonic acid, $\tau_{COOH} = 0.12 \pm 0.03$ $\mu$s was obtained at 25 °C from measurements of the $^1$H relaxation induced by proton-exchange modulation of the $^1H-^{17}O$ scalar spin coupling and assuming a cyclic exchange mechanism involving two water molecules.[38] A factor of ~2 difference between these results can be attributed to the kinetic H/D isotope effect[38] and to the 15 °C temperature difference.

The pH dependence of the OD contribution is entirely due to acid-catalyzed hydrogen exchange, as described by the rate constant $k_1^{OD}$ in eq 8. At pH* 5.4 and 7.4, this process is negligible compared to the direct mechanism (described by $k_0^{OD}$). The low-frequency OD contribution to $R_1$ thus drops from 15 $s^{-1}$ at pH* 3.1 to 12 $s^{-1}$ at pH* 4.2 and ~2.5 $s^{-1}$ at pH* 5.4 and 7.4. The rate constants obtained from the fit in Figure 4a, $k_0^{OD} = (2.8 \pm 0.1) \times 10^3$ $s^{-1}$ and $k_1^{OD} = (4.6 \pm 0.1) \times 10^7$ $M^{-1}$ $s^{-1}$ (in $D_2O$ at 10 °C), are similar to the values, $k_0^{OH} = 1.4 \times 10^3$ $s^{-1}$ and $k_1^{OH} = 3 \times 10^7$ $M^{-1}$ $s^{-1}$ (in $H_2O$ at 25 °C), for OH in glucose[48] and to the value, $k_1^{OH} = 4 \times 10^7$ $M^{-1}$ $s^{-1}$ (in $H_2O$ at 4 °C), for Ser and Thr in tetrapeptides.[49] While a direct mechanism is not evident for Ser and Thr and is not firmly established even for glucose, it might operate in the collagen triple helix by making use of the crystallographically identified[5] (but short-lived) water bridges involving Hyp residues in the triple helix (Hyp accounts for 58% of all OH groups in our gelatin; see Table 1). Fits with $k_0^{OD} = 0$ yield unphysical water and OD parameters, but the COOD parameters are hardly affected.

The local side-chain order parameter is twice as high for OD groups ($S_{OD} = 0.71$) as for COOD groups ($S_{COOD} = 0.35$). This difference can be understood in terms of the conformational flexibility associated with side-chain rotamers. The OD class is dominated by Hyp (58%), Ser (25%), and Thr (10%), with one, two, and two, respectively, single bonds between the α carbon and the hydroxyl deuteron. Hence we can expect a relatively large order parameter. The COOD class consists of Glu (62%) and Asp (38%) with four and three, respectively, single bonds between the α carbon and the carboxyl deuteron. Hence the COOD class should have a smaller order parameter than the OD class, as observed. The $^2$H order parameters obtained here are similar to the value, $S_{OD} = 0.50 \pm 0.05$, deduced from $^2$H MRD data for the small globular protein bovine pancreatic trypsin inhibitor.[36] This value is an rms average over five COOD and eight OD groups (dominated by Tyr and with no Hyp). This order parameter describes the effect of local orientational averaging on time scales shorter than the protein rotational correlation time of ~5 ns. In the gelatin gel, the order parameters are averaged over the much longer residence times of labile deuterons, which are in the range 0.3 $\mu$s−0.4 ms at the investigated pH values. The finding of similar order parameters in the two cases indicates that most of the orientational averaging takes place on nanosecond or shorter time scales.

For the fraction, $x_{helix} = 1 - x_{strand}$, of OD groups in ordered triple-helical segments, the fit yields 77 ± 2% (Table 2). Since the OD groups should be uniformly distributed between ordered and disordered segments, the quantity $x_{helix}$ can be regarded as the overall fraction of amino acid residues in triple-helical segments. This value is somewhat higher than what has been found (up to 65%) by polarimetry after annealing 4.5% gelatin gels for 15 h at 10 °C.[13] The difference may be due to the higher gelatin concentration (10%) in our samples and/or to differences in the gelatin preparations or gel setting and annealing protocol. The relatively small order parameter obtained for single-strand segments, $S_{strand} = 0.11 \pm 0.02$, implies considerable conformational flexibility on the microsecond time scale. This is not unreasonable for the many loose, dangling ends that are thought to be present in the gel.[2,14] Some hydrolyzed polypeptide fragments may also contribute to the single-strand fraction. Furthermore, the local order parameter $S_{OD}$ might be smaller in single-strand segments than in triple helices, and this would lower the apparent $S_{strand}$.

**3.3. Dynamics of Hydration Water.** The five pH-independent water parameters in Table 2 describe three classes of hydration water: mobile surface waters with correlation times < 1 ns, and two groups of trapped water molecules with residence times $\tau_{W1} = 3.6 \pm 0.4$ ns and $\tau_{W2} = 39 \pm 3$ ns. These long-lived water molecules must be responsible for the $^{17}$O dispersions in Figure 3. We therefore performed bilorentzian fits to the $^{17}$O data with the two correlation times fixed at the values obtained from the $^2$H fit. As anticipated, the $^{17}$O profiles can be reproduced with these correlation times, and the values of the three adjustable parameters do not depend significantly on pH. In the following, we compare the $^2$H and $^{17}$O amplitude parameters, using for $^{17}$O the average of the parameters obtained at pH* 4.2 and 5.4 (since pH* 8.5 is outside the pH* range analyzed for $^2$H).

When combined with the known values of $R_1^{(0)}$ and $N_T$ (section 2), the mobile surface water parameter α yields the quantity $N_S(\langle\tau_S\rangle/\tau_{bulk} - 1)$.[21] Here, $N_S$ is the average number of water molecules interacting with an amino acid residue in gelatin, and $\langle\tau_S\rangle$ is their average rotational correlation time. The $^2$H data yield $N_S(\langle\tau_S\rangle/\tau_{bulk} - 1) = 19.5 \pm 0.5$, and the corresponding $^{17}$O value is 25 ± 5% larger. These values are about twice as large as expected for a fully exposed polypeptide chain with a typical amino acid sequence,[50−52] despite the fact that the backbone is not fully exposed in the gelatin gel. On the basis of solvent-accessible surface area calculations, we estimate that $N_S \approx 5$. The MRD results then translate into a rotational retardation factor, $\langle\tau_S\rangle/\tau_{bulk} \approx 5$, significantly higher than the values of 2−3 deduced for fully exposed amino acids[50,51] but similar to the average value for globular proteins, $\langle\tau_S\rangle/\tau_{bulk} = 5.4 \pm 0.6$, at 27 °C.[22] For globular proteins, the rotational retardation factor is thought to be dominated by a small number of water molecules in deep surface pockets.[19−22,52] Although there are no deep pockets in the collagen triple helix, a similar role might be played by the polar helical groove (Figure 1) containing the crystallographically inferred H-bonded water bridges.[5] Furthermore, the surface of the collagen triple helix appears to be less polar than the surface of a typical globular protein, and nonpolar atoms are known to give the largest rotational retardation.[20,50]

For the amplitude parameters, the fits to the $^{17}$O data (Figure 3) yield $N_{W1}S_{W1}^2 = (4.0 \pm 0.3) \times 10^{-2}$ for the 3.6-ns component and $N_{W2}S_{W2}^2 = (2.4 \pm 0.3) \times 10^{-3}$ for the 39-ns component. These values correspond to at least (for $S_W = 1$) one 3.6-ns water molecule per 25 residues and at least one 39-

ns water molecule per 420 residues. There are no cavities or deep pockets in the collagen triple helix (Figure 1), so these long-lived water molecules must be located in irregular transition zones between triple-helical and single-strand segments in the gel network or in structural defects within triple-helical regions. Triple helices in the gel are thought[15] to be nucleated from two polypeptide chains, one of which doubles back on itself, so the triple-helical segments in the gel must deviate locally from the idealized collagen triple helix structure and such defects may produce cavities or other hydration sites that could give rise to long water residence times. The typical length of a triple-helical segment is 100−200 residues in each strand,[15] so the 39-ns component corresponds roughly to one highly ordered water molecule per triple-helical segment. The most long-lived water molecules may therefore be associated with the irregular transition zones where the triple helix branches out in several strands. The 3.6-ns component corresponds to 12−24 water molecules per triple-helical segment and is thus more likely to be associated with defects within the triple helix.

From the ratio of the $^{17}$O and $^{2}$H $N_{W,k}S_{W,k}^2$ parameters, we can calculate the $^{17}$O/$^{2}$H order parameter ratio (since $N_{W,k}$ cancels out). We thus obtain $S_{W,k}(^{17}O)/S_{W,k}(^{2}H) = 1.2 \pm 0.1$ and $0.8 \pm 0.1$ for the 3.6-ns and 39-ns components, respectively. The small but significant deviations of these ratios from unity indicates that the long-lived water molecules undergo anisotropic local motions during their residence time. For example, a fast 180° flip about the $C_2$ water axis (without any librations) would give an order parameter ratio of 1.64, whereas a 30° twist libration about the $C_2$ axis (without any flips) would give a ratio of 0.74.[21]

**3.4. Exchange of OD and ND Deuterons at Basic pH.** The pH dependence of the $^{2}$H profiles on the basic side primarily reflects the base-catalyzed exchange of OD and ND deuterons in amino acid side chains. The model must therefore be supplemented with two rate constants, $k_2^{OD}$ and $k_2^{ND}$, and one order parameter, $S_{ND}$. However, this model cannot reproduce the pH dependence in the 1−100 MHz range, which is evident at pH* 8.6 and 9.4 but not at lower pH* values (Figures 2 and 5a). Hydrogen exchange with OD or ND groups cannot give rise to (apparent) correlation times much shorter than 1 $\mu$s ($\approx 1/\Omega_{OD/ND}$), so this pH-dependent MHz dispersion must have a different origin. Since this contribution increases markedly with pH* (Figure 2) and is seen in the $^{2}$H profiles but not in the $^{17}$O profiles (Figure 3), it must be attributed to labile deuterons rather than to long-lived water molecules. Furthermore, because this contribution is not seen at pH* 3.1, it must be due to local reorientation of N−D vectors in Arg, Lys, and Hyl (hydroxylysine) side chains. A significant contribution from internal motions in these long and flexible side chains is consistent with the small order parameter $S_{ND}$ deduced from the fit (see below). Two correlation times, $\tau_{int,1}$ and $\tau_{int,2}$, are needed to model this contribution adequately. The correlation times, but not the corresponding effective amplitude parameters, $N_{int,1}$ and $N_{int,2}$, were constrained to be the same at both pH* values.

The simultaneous fit to the pH* 8.6 and 9.4 profiles (98 $R_1$ values) is shown in Figure 5a and the resulting values of the nine adjustable parameters (six of which are associated with the high-frequency internal motion) are given in Table 3. Unsuccessful attempts were made to improve the fit below 10 kHz by introducing distinct order parameters for ND deuterons in Arg and Lys side chains. The fit to this data set is challenging because the internal-motion dispersion (with one correlation time on the order of $10^{-7}$ s) overlaps with the OD dispersion which, in turn, overlaps with the ND dispersion (Figure 5b).

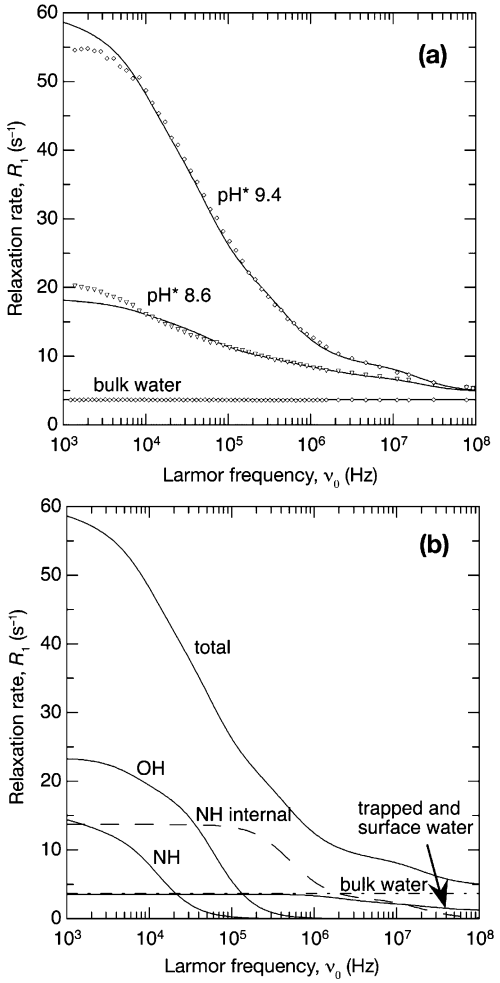


**Figure 5.** (a) $^{2}$H MRD profiles from gelatin gels at 10.0 °C and the indicated basic pH* values, all scaled to a concentration of 60 water molecules per amino acid residue. The dispersion curves resulted from a simultaneous fit to all data (see text). The parameter values resulting from the fit are given in Table 3. (b) Decomposition of the pH* 9.4 dispersion profile, showing the contributions from deuterons in hydration water molecules and in gelatin Arg, Lys, and Hyl (NH) and hydroxyl (OH) groups.

**TABLE 3: Results of Simultaneous Fit to Two $^{2}$H Profiles at pH* 8.6 and 9.4**

| parameter (unit) | value |
|---|---|
| $N_{int,1}$(pH* 8.6) | $(2.9 \pm 0.1) \times 10^{-2}$ |
| $N_{int,1}$(pH* 9.4) | $(7.9 \pm 0.2) \times 10^{-2}$ |
| $\tau_{int,1}$ (ns) | $4.5 \pm 0.2$ |
| $N_{int,2}$(pH* 8.6) | $(1.3 \pm 0.1) \times 10^{-3}$ |
| $N_{int,2}$(pH* 9.4) | $(7.9 \pm 0.2) \times 10^{-3}$ |
| $\tau_{int,2}$ ($\mu$s) | $0.17 \pm 0.01$ |
| $k_2^{OD}$ (M$^{-1}$ s$^{-1}$) | $(1.3 \pm 0.1) \times 10^{10}$ |
| $k_2^{ND}$ (M$^{-1}$ s$^{-1}$) | $(4.5 \pm 0.2) \times 10^{9}$ |
| $S_{ND}$ | $0.17 \pm 0.01$ |

Considering now the parameter values in Table 3, we note that $S_{ND}$ has the small magnitude expected for flexible Arg and Lys side chains. The rate constants $k_2^{OD}$ and $k_2^{ND}$ are both on the order of $10^{10}$ M$^{-1}$ s$^{-1}$, as expected for diffusion-controlled base-catalyzed hydrogen exchange.[53] The diffusion-controlled bimolecular rate constant for noninteracting molecules with a distance of closest approach $\sigma$ is $k_{diff} = 4\pi\sigma D_{rel}$. Inserting the (apparent) diffusion coefficient of $OD^-$ in $D_2O$ at 10 °C, $D_{OD} \approx 2 \times 10^{-9}$ m$^2$ s$^{-1}$, and the solvated triple-helix radius, $\sigma \approx 10$ Å, we obtain $k_{diff} \approx 1.5 \times 10^{10}$ M$^{-1}$ s$^{-1}$. From NMR measurements on free Arg in $H_2O$ at 25 °C, values of $k_2^{NH} = 4 \times 10^9$ M$^{-1}$ s$^{-1}$ for $\eta$-NH and $1 \times 10^{10}$ M$^{-1}$ s$^{-1}$ for $\epsilon$-NH have been reported,[54]

and CPMG measurements on BPTI yielded (in $H_2O$ at 27 °C) $k_2^{NH} = 2.1 \times 10^9$ $M^{-1}$ $s^{-1}$ for $\eta$-NH and $9 \times 10^8$ $M^{-1}$ $s^{-1}$ for $\epsilon$-NH in Arg and $3.9 \times 10^{10}$ $M^{-1}$ $s^{-1}$ for Lys.[55] For Ser and Thr in tetrapeptides, $k_2^{OH} = (4-6) \times 10^9$ $M^{-1}$ $s^{-1}$ was obtained[49] in $H_2O$ at 4 °C, and for glucose in $H_2O$ at 23 °C, $k_2^{OH} = 6 \times 10^9$ $M^{-1}$ $s^{-1}$ was reported.[48] In conclusion, our $k_2^{OD}$ and $k_2^{ND}$ values are slightly larger than most literature values, but this may be attributed to the high solvent exposure of side chains in the triple helix.

The five internal motion parameters in Table 3 cannot be interpreted in detail. However, the amplitude parameters are consistent with Arg and Lys ND deuterons being responsible for this contribution (Table 1). The pH dependence of the amplitude parameters can be understood as an effect of intermediate exchange. With $k_2^{ND}$ from Table 3 in eq 10, $\tau_{ND}$ decreases from 2 ms at pH* 8.6 to 0.3 ms at pH* 9.4. These values are not short compared to the zero-frequency intrinsic relaxation time associated with internal motions, which can be estimated as $T_{int,k}(0) = [(^3/_2)(\pi\chi_{ND})^2\tau_{int,k}]^{-1} \approx 0.5$ ms and 10 $\mu$s for components 1 and 2, respectively. Therefore, neither component is fully in the fast-exchange limit even at pH* 9.4.

**3.5. Comparison with Previous NMR Relaxation Studies.** Numerous water $^1H$ and $^2H$ NMR studies of collagen fibrils from tendon and cartilage have been performed over the past four decades. Because of the fibrillar superstructure and the low water content in such samples, meaningful comparisons are not easily made with the present study of dilute gelatin gels. Early measurements of dipolar and quadrupolar splittings from water in collagen fibrils were interpreted in terms of specific hydration geometries.[56-60] Other studies have examined the relative importance of hydrogen exchange and dipolar cross-relaxation for $^1H$ magnetization transfer in collagen fibrils.[61-69] Rotating-frame ($T_1\rho$) $^1H$ relaxation dispersions in the kHz range have also been measured in tendon and cartilage and interpreted in terms of hydrogen-exchange modulated chemical shifts.[31,70] This relaxation mechanism does not contribute to the (laboratory-frame) $R_1$ dispersion.

Like collagen fibrils, gelatin gels have been investigated by magnetic relaxation techniques since the early days of NMR.[71,72] Notably, $^1H$ dispersion profiles (covering more than four frequency decades) from gelatin gels were reported already in 1970, but a quantitative interpretation was not attempted.[73,74] More recently, several high-frequency (20−400 MHz) $^1H$ relaxation studies of water in gelatin gels have appeared.[12,28,75-78] The focus in most of these studies has been on the CPMG pulse-train dispersion of $T_2$, caused by variations in the $^1H$ chemical shift on the millisecond time scale and variously attributed to exchange with labile gelatin protons[28] or to water diffusion through local magnetic field gradients.[78] Because the accessible frequency window is relatively narrow, the CPMG technique only detects proton exchange on the millisecond time scale. It is therefore difficult to separate contributions from different labile proton classes, unless dispersions are recorded at many pH values.[55] On the basis of CPMG data, it has been concluded that the number of exchanging polypeptide protons is reduced by a factor of 2−3 on gelation.[28,78] However, all side chains are fully exposed in the collagen triple helix[4-7] and this should be approximately true also for the imperfect triple helices in the gelatin gel.

The dynamics of the crystallographically inferred water bridges at the surface of the triple helix[5] have been explored in an intermolecular NOE study of a collagen-like triple helix in solution.[18] It has subsequently been shown that this technique suffers from long-range dipolar artifacts, precluding characterization of subnanosecond hydration dynamics.[52,79] However, sufficiently long-lived (≥ nanoseconds) water molecules can be detected, but the NOE study found no evidence for such long-lived hydration structures at 5 °C.[18] This negative finding is consistent with the present MRD results, showing that the long-lived water molecules in gelatin gels are few and presumably associated with structural defects. A collagen triple helix without such defects does not have the internal cavities or deep surface pockets required to trap water molecules.

## 4. Conclusions

We have presented $^2H$ and $^{17}O$ MRD profiles from aqueous gelatin gels, covering five frequency decades (for $^2H$) and six pH values. This extensive data set was globally analyzed in terms of a recently developed theory[24] for nuclear spin relaxation induced by hydrogen or water exchange between anisotropic sites in a rotationally immobilized polymer and an abundant bulk solvent phase. The $^2H$ and $^{17}O$ dispersion profiles at all pH values could be quantitatively reproduced with a model featuring two classes of long-lived (trapped) water molecules and three classes of labile deuterons (COOD, OD, and ND). In this model, hydrogen or water exchange does not merely average spatial heterogeneities in relaxation rates but actually causes spin relaxation. In other words, the residence times (or inverse exchange rates) are the relevant correlation times for the nuclear quadrupole interaction that induces spin−lattice relaxation. Under such conditions, the motional-narrowing regime becomes synonymous with the fast-exchange regime. The conventional perturbation theory of spin relaxation[23] therefore breaks down under conditions of slow or intermediate exchange. This is the case for the OD and ND labile deuteron classes, for which the generalized relaxation theory predicts that the dispersion occurs at the (residual) quadrupole frequency, while the correlation (exchange) time plays the role of a scaling factor.

The parameter values emerging from the global analysis are consistent with the available reference data for small molecules. For the carboxyl groups in Asp and Glu side chains, the acid dissociation constant has the expected value $pK_{COOH} = 4.25$ (after H/D isotope correction). All five hydrogen-exchange rate constants in the model have values consistent with small-molecule data. The orientational order parameters of the labile deuterons in the highly solvent-exposed side chains decrease in the order $S_{OD} = 0.71 > S_{COOD} = 0.35 > S_{ND} = 0.17$, as expected if conformational flexibility is mainly governed by the (average) number of single bonds between the α carbon and the labile deuteron, calculated from the amino acid composition to be 1.5 > 3.6 > 4.2. The strong observed pH dependence in the $^2H$ dispersion profiles can thus be rationalized quantitatively with physically reasonable parameters and a rigorous relaxation theory.

The analysis of the $^2H$ and $^{17}O$ MRD profiles also yields a dynamic characterization of hydration in gelatin gels. Our data show that the H-bonded water bridges seen in crystal structures of collagen-like triple helices are highly mobile. On average, water motions in the hydration layer are retarded by a factor of ∼5 as compared to bulk water. This is consistent with the view, based primarily on previous MRD studies and MD simulations of globular proteins,[22] that surface topology (rather than hydrogen bonding) is the main determinant of hydration dynamics. The $^2H$ and $^{17}O$ dispersions seen above ∼1 MHz are produced by a small number of water molecules trapped in the gelatin structure for periods of 4−40 ns at 10 °C. These long-lived water molecules do not correspond to water bridges on the exposed surface of the triple helix but are associated

with structural defects and branch points in the gel network. The MRD data also show that 23% of the gelatin residues do not form rigid triple helices but belong to single-strand segments, whose low order parameter, $S_{strand} = 0.11$, indicates substantial flexibility.

As shown elsewhere,[25] the $^1$H MRD profiles from gelatin gels can be rationalized along the same lines, using a generalized relaxation theory appropriate for dipolar spin relaxation and taking magnetic cross-relaxation into account.[33] The analysis of the present $^2$H and $^{17}$O MRD data is more straightforward, since these quadrupolar nuclides are relaxed by a single-spin mechanism. The present results therefore serve as benchmarks for the subsequent analysis of $^1$H MRD data from the same system, thereby helping to clarify the molecular basis for the relaxation phenomena that underlie much of the clinical applications of magnetic resonance imaging.

**Acknowledgment.** We thank Karim Snoussi and Hans Lilja for experimental assistance. This work was supported by the Swedish Research Council and the Knut and Alice Wallenberg Foundation.

## References and Notes

(1) van der Rest, M.; Garrone, R. *FASEB J.* **1991**, *5*, 2814−2823.
(2) te Nijenhuis, K. *Adv. Polym. Sci.* **1997**, *130*, 160−193.
(3) Brodsky, B.; Persikov, A. V. *Adv. Protein Sci.* **2005**, *70*, 301−339.
(4) Bella, J.; Eaton, M.; Brodsky, B.; Berman, H. M. *Science* **1994**, *266*, 75−81.
(5) Bella, J.; Brodsky, B.; Berman, H. M. *Structure* **1995**, *3*, 893−906.
(6) Kramer, R. Z.; Venugopal, M. G.; Bella, J.; Mayville, P.; Brodsky, B.; Berman, H. M. *J. Mol. Biol.* **2000**, *301*, 1191−1205.
(7) Berisio, R.; Vitagliano, L.; Mazzarella, L.; Zagari, A. *Protein Sci.* **2002**, *11*, 262−270.
(8) Ramachandran, G. N.; Bansal, M.; Bhatnagar, R. S. *Biochim. Biophys. Acta* **1973**, *322*, 166−171.
(9) Suzuki, E.; Fraser, R. D. B.; McRae, T. P. *Int. J. Biol. Macromol.* **1980**, *2*, 54−56.
(10) Holmgren, S. K.; Taylor, K. M.; Bretscher, L. E.; Raines, R. T. *Nature* **1998**, *392*, 666−667.
(11) Djagny, K. B.; Wang, Z.; Xu, S. *Crit. Rev. Food Sci. Nutr.* **2001**, *41*, 481−492.
(12) Djabourov, M.; Leblond, J.; Papon, P. *J. Phys. (Paris)* **1988**, *49*, 319−332.
(13) Joly-Duhamel, C.; Hellio, D.; Djabourov, M. *Langmuir* **2002**, *18*, 7208−7217.
(14) Harrington, W. F.; Rao, N. V. *Biochemistry* **1970**, *9*, 3714−3724.
(15) Benguigui, L.; Busnel, J.-P.; Durand, D. *Polymer* **1991**, *32*, 2680−2685.
(16) Guo, L.; Colby, R. H.; Lusignan, C. P.; Howe, A. M. *Macromolecules* **2003**, *36*, 10009−10020.
(17) Pezron, I.; Djabourov, M.; Bosio, L.; Leblond, J. *J. Polym. Sci., Part B: Polym. Phys.* **1990**, *28*, 1823−1839.
(18) Melacini, G.; Bonvin, A. M. J. J.; Goodman, M.; Boelens, R.; Kaptein, R. *J. Mol. Biol.* **2000**, *300*, 1041−1048.
(19) Denisov, V. P.; Halle, B. *Faraday Discuss.* **1996**, 103, 227−244.
(20) Halle, B. In *Hydration Processes in Biology*; Bellisent-Funel, M.-C., Ed.; IOS Press: Dordrecht, 1998; pp 233−249.
(21) Halle, B.; Denisov, V. P.; Venu, K. In *Biological Magnetic Resonance*; Krishna, N. R., Berliner, L. J., Eds.; Kluwer/Plenum: New York, 1999; Vol. 17, pp 419−484.
(22) Halle, B. *Philos. Trans. R. Soc. London B* **2004**, *359*, 1207−1224.
(23) Abragam, A. *The Principles of Nuclear Magnetism*; Clarendon Press: Oxford, 1961.
(24) Halle, B. *Prog. NMR Spectrosc.* **1996**, *28*, 137−159.
(25) Vaca Chávez, F.; Halle, B. *Magn. Reson. Med.* **2006**, *56*, 73−81.
(26) Gore, J. C.; Brown, M. S.; Zhong, J.; Mueller, K. F.; Good, W. *Magn. Reson. Med.* **1989**, *9*, 325−332.
(27) Ceckler, T. L.; Wolff, S. D.; Yip, V.; Simon, S. A.; Balaban, R. S. *J. Magn. Reson.* **1992**, *98*, 637−645.
(28) Hills, B. P. *Mol. Phys.* **1992**, *76*, 509−523.
(29) Koenig, S. H.; Brown, R. D. In *Encyclopedia of Nuclear Magnetic Resonance*; Grant, D. M., Harris, R. K., Eds.; Wiley: New York, 1996; pp 4108−4120.
(30) Liepinsh, E.; Otting, G. *Magn. Reson. Med.* **1996**, *35*, 30−42.
(31) Duvvuri, U.; Goldberg, A. D.; Kranz, J. K.; Hoang, L.; Reddy, R.; Wehrli, F. W.; Wand, A. J.; Englander, S. W.; Leigh, J. S. *Proc. Natl. Acad. Sci. U.S.A.* **2001**, *98*, 12479−12484.
(32) Korb, J.-P.; Bryant, R. G. *Magn. Reson. Med.* **2002**, *48*, 21−26.
(33) Halle, B. *Magn. Reson. Med.* **2006**, *56*, 60−72.
(34) Noack, F. *Prog. NMR Spectrosc.* **1986**, *18*, 171−276.
(35) Ferrante, G.; Sykora, S. *Adv. Inorg. Chem.* **2005**, *57*, 405−470.
(36) Denisov, V. P.; Halle, B. *J. Mol. Biol.* **1995**, *245*, 698−709.
(37) Luz, Z.; Meiboom, S. *J. Am. Chem. Soc.* **1963**, *85*, 3923−3925.
(38) Lankhorst, D.; Schriever, J.; Leyte, J. C. *Chem. Phys.* **1983**, *77*, 319−340.
(39) Covington, A. K.; Paabo, M.; Robinson, R. A.; Bates, R. G. *Anal. Chem.* **1968**, *40*, 700−706.
(40) Covington, A. K.; Robinson, R. A.; Bates, R. G. *J. Phys. Chem.* **1966**, *70*, 3820−3824.
(41) Kenchington, A. W.; Ward, A. G. *Biochem. J.* **1954**, *58*, 202−207.
(42) Laughton, P. M.; Robertson, R. E. In *Solute−Solvent Interactions*; Coetzee, J. F., Ritchie, C. D., Eds.; M. Dekker: New York, 1969; pp 399−538.
(43) van Slyke, D. D.; Hiller, A.; MacFadyen, D. A.; Hastings, A. B.; Klemperer, F. W. *J. Biol. Chem.* **1940**, *133*, 287−288.
(44) Press, W. H.; Teukolsky, S. A.; Vetterling, W. T.; Flannery, B. P. *Numerical Recipes in C*, 2nd ed.; Cambridge University Press: Cambridge, 1992
(45) Schowen, K. B.; Schowen, R. L. *Methods Enzymol.* **1982**, *87*, 551−606.
(46) Forsyth, W. R.; Antosiewicz, J. M.; Robertson, A. D. *Proteins* **2002**, *48*, 388−403.
(47) Harned, H. S.; Ehlers, R. W. *J. Am. Chem. Soc.* **1933**, *55*, 652−656.
(48) Hills, B. P. *Mol. Phys.* **1991**, *72*, 1099−1121.
(49) Liepinsh, E.; Otting, G.; Wüthrich, K. *J. Biomol. NMR* **1992**, *2*, 447−465.
(50) Ishimura, M.; Uedaira, H. *Bull. Chem. Soc. Jpn.* **1990**, *63*, 1−5.
(51) Denisov, V. P.; Jonsson, B.-H.; Halle, B. *Nat. Struct. Biol.* **1999**, *6*, 253−260.
(52) Modig, K.; Liepinsh, E.; Otting, G.; Halle, B. *J. Am. Chem. Soc.* **2004**, *126*, 102−114.
(53) Eigen, M. *Angew. Chem., Int. Ed.* **1964**, *3*, 1−19.
(54) Henry, G. D.; Sykes, B. D. *J. Biomol. NMR* **1995**, *5*, 59−66.
(55) Denisov, V. P.; Halle, B. *J. Am. Chem. Soc.* **2002**, *124*, 10264−10265.
(56) Berendsen, H. J. C. *J. Chem. Phys.* **1962**, *36*, 3297−3305.
(57) Chapman, G. E.; McLauchlan, K. A. *Proc. R. Soc. London B* **1969**, *173*, 223−234.
(58) Dehl, R. E.; Hoeve, C. A. J. *J. Chem. Phys.* **1969**, *50*, 3245−3251.
(59) Fung, B. M.; Trautmann, P. *Biopolymers* **1971**, *10*, 391−397.
(60) Migchelsen, C.; Berendsen, H. J. C. *J. Chem. Phys.* **1973**, *59*, 296−305.
(61) Fung, B. M.; Witschel, J.; McAmis, L. L. *Biopolymers* **1974**, *13*, 1767−1776.
(62) Edzes, H. T.; Samulski, E. T. *Nature* **1977**, *265*, 521−523.
(63) Edzes, H. T.; Samulski, E. T. *J. Magn. Reson.* **1978**, *31*, 207−229.
(64) Fung, B. M.; McGaughy, T. W. *J. Magn. Reson.* **1980**, *39*, 413−420.
(65) Tzou, D.-L.; Lee, S.-M.; Yeung, H. N. *Magn. Reson. Med.* **1997**, *37*, 359−365.
(66) Eliav, U.; Navon, G. *J. Magn. Reson.* **1999**, *137*, 295−310.
(67) Lattanzio, P.-J.; Marshall, K. W.; Damyanovich, A. Z.; Peemoeller, H. *Magn. Reson. Med.* **2000**, *44*, 840−851.
(68) Navon, G.; Shinar, H.; Eliav, U.; Seo, Y. *NMR Biomed.* **2001**, *14*, 112−132.
(69) Eliav, U.; Navon, G. *J. Am. Chem. Soc.* **2002**, *124*, 3125−3132.
(70) Virta, A.; Komu, M.; Kormano, M. *Magn. Reson. Med.* **1997**, *37*, 53−57.
(71) Balazs, E. A.; Bothner-By, A. A.; Gergely, J. *J. Mol. Biol.* **1959**, *1*, 147−154.
(72) Odeblad, E. *Nature* **1960**, *188*, 579.
(73) Kimmich, R.; Noack, F. *Z. Naturforsch.* **1970**, *25a*, 299−301.
(74) Kimmich, R.; Noack, F. *Z. Naturforsch.* **1970**, *25a*, 1680−1684.
(75) Maquet, J.; Theveneau, H.; Djabourov, M.; Leblond, J.; Papon, P. *Polymer* **1986**, *27*, 1103−1110.
(76) Hills, B. P.; Favret, F. A. *J. Magn. Reson. B* **1994**, *103*, 142−151.
(77) Vackier, M.-C.; Hills, B. P.; Rutledge, D. N. *J. Magn. Reson.* **1999**, *138*, 36−42.
(78) Traoré, A.; Foucat, L.; Renou, J.-P. *Eur. Biophys. J.* **2000**, *29*, 159−164.
(79) Halle, B. *J. Chem. Phys.* **2003**, *119*, 12372−12385.